Adhesion anisotropy between contacting electrospun fibers

Urszula Stachewicz[1,2], Fei Hang[2,†] and Asa H. Barber[1,2]*

[1]Nanoforce Technology Ltd., Queen Mary University of London, Mile End Road, London E1 4NS, United Kingdom

[2]Department of Materials, School of Engineering and Materials Science, Queen Mary University of London, Mile End Road, London E1 4NS, United Kingdom

KEYWORDS

Adhesion, Fibers, electrospinning, Polyamide 6, Nylon 6,

ABSTRACT

The mechanical properties of electrospun fiber networks are critical in a range of applications from filtration to tissue engineering and are dependent on the adhesion between contacting fibers within the network. This adhesion is complex as electrospun networks exhibit a variety of contacts, including both cross-cylinder and parallel fiber configurations. *In situ* atomic force microscopy (AFM) was used to quantify the work of adhesion between a pair of individual

electrospun polyamide fibers using controlled orientations and measurable contact areas. The work of adhesion was found to depend strongly on the fiber-fiber contact, with separation of fibers in a parallel fiber configuration exhibiting considerably higher work of adhesion across a range of contact lengths than a cross-cylinder configuration. Our work therefore highlights direction dependent adhesion behavior between electrospun fibers due a suggested polymer chain orientation mechanism, which increases net van der Waals interactions and indicates variability of adhesion within a random electrospun fiber network.

INTRODUCTION

Nonwoven fibers produced from electrospinning are used extensively as 2D in-plane networks for filtration membranes[1] and medical applications such as tissue scaffolds.[2,3] The resultant mechanical properties of these networks are critically defined by the adhesion between contacting fibers, which often acts at relatively small length scales due to the sub-micron diameters of the electrospun fibers within the network. The importance of electrospun fiber applications has led to studies that attempt to understand adhesion behavior within the network including through molecular dynamic simulations of fiber-fiber interactions.[4] Further work has quantified the adhesion between individual polymer fibers using a low load tensile tester to separate contacting electrospun fibers in a cross-cylinder configuration, with the dependence of fiber diameter and roughness on adhesion investigated.[5] A more recent study further showed the effect of environmental conditions and molecular orientation on the adhesion between contacting electrospun fibers.[6] The characterization of freestanding nanofibers has been additionally investigated using a nano-cheese-cutter to determine both the elastic modulus of the electrospun

fibers and their adhesion strength, again using a cross-cylinder configuration.[7] Such investigations generally found a measured adhesion strength in the range corresponding to typical van der Waals forces, which also exhibited a linear relationship between the force required to separate the two fibers, known as the 'pull-off' force, and the fiber radius.[5] However, the contact between fibers was fixed towards a cross-cylinder configuration where a relatively small fiber-fiber contact area was examined. The adhesion between fibers measured using a cross-cylinder configuration is effective at describing the interfiber adhesion when forces act to separate fibers within the resultant electrospun fiber network, but does not describe fiber-fiber interactions when forces are acting in the plane of the electrospun fiber network as described in previous literature.[3-5,8] Specific surface properties of electrospun fibers introduced from the spinning process have been highlighted as differing from bulk polymer surface behavior[8,9] and will define the adhesion between contacting fibers in the network in addition to the resultant contact area. Further non-bulk behavior has been justified from structural arguments based on supramolecular confinement within the electrospun fiber to give, for example, increases in the fiber elastic modulus with decreasing fiber diameter.[10] Importantly, other fibrous networks ranging from the relatively small 'spatula-like' fibers found on the foot of the gecko, to gecko-inspired synthetic adhesives[11] and microfiber arrays have displayed adhesion that is depending on the direction of contacting fibers. For example, direction dependent anisotropic adhesion is observed in the fibrous setal arrays of the gecko foot and is used to increase and decrease the adhesive contact between the foot and a surface as the gecko moves over a surface.[9] Such adhesion mechanisms found in biology have been exploited synthetically using arrays of polypropylene fibers and a glass substrate, which showed that sliding along the principal fiber

axis direction produces much higher shear force relative to other directions and is attributed to increased contact area that subsequently caused fibers bending.[8]

The adhesion properties of electrospun fibrous materials is often visualized using wetting experiments and contact angle measurements.[12] Controlled wetting of electrospun fiber membranes has been successfully achieved using a number of methods including coating with hydrophobic polymerized perfluoroalkyl ethyl methacrylate, using initiated chemical vapor deposition, adding hierarchical roughness by controlling fiber morphology and introducing high density of relatively small diameter beads into the membrane.[13] However, electrospun fiber membrane applications such as filtration and tissue engineering, where transport phenomena and adhesion are important, require enhance wettability between the liquid media and electrospun fiber surfaces. Increasing wettability can be also performed by modifying surface chemistry, such as adsorption of soya proteins onto polypropylene (PP) nonwoven surfaces to provide enhanced hydrophylicity.[14]

Understanding both the adhesion and potential direction dependence between electrospun fibers in a network is therefore critical in both understanding the properties of electrospun fiber networks and developing improved network structures. The aim of this study is to understand the properties of electrospun fiber networks by measuring the adhesion between fibers in a number of configurations based on both a cross-cylinder contact, as has been carried out previously, while additional in-plane separations of contacting fibers indicative of more typical deformations mechanisms in electrospun fiber applications is explored. Understanding the adhesion between fibers in an electrospun network critically requires quantitative evaluation of the orientation

between pairs of contacting fibers that define the resultant contact area. Figure 1 shows a typical electrospun network and highlights the random orientation of fibers within this network. The cross-cylinder configuration between fibers at an angle of 90˚ provides the minimum contact area between fibers, which is rarely observed in the case of the randomly oriented electrospun mesh of fibers in Figure 1. Higher resolution imaging using transmission electron microscopy (TEM) in Figure 2 details the contact between electrospun fibers and indicates, as expected, an increase in the contact area as the orientation of fibers around the contact point deviates from 90˚. Furthermore, 3D imaging of electrospun networks has shown that the deposition of fibers onto a flat substrate during the electrospinning process causes random orientation of fibers within layered planes parallel to the plane of the substrate.[15] The electrospun fibers will slide over one another in the plane of the network during, for example, fluid flow through an electrospun network in filtration causing a pressure difference that deforms the electrospun fiber network through bending. Tensile and compressive deformation of a network in bending results in a range of fiber deformation mechanisms from fiber extension and compression as well as, critically, sliding between the contacting fibers in the network.[16] Such sliding of fibers over one another is also important in defining the extensibility, or tortuosity, of fibers in the network for the simulation of soft tissues.[17] The adhesion between electrospun fibers within the network structure should therefore be evaluated through separation of the fibers along their principal axis.

Previous work has utilized experimental techniques to apply forces to individual electrospun fibers using atomic force microscope (AFM) in combination with scanning electron microscope (SEM). Such an experimental setup is powerful in examining deformation mechanisms for individual fibers with sub-micron diameters *in situ* using SEM while AFM gives force

information. The mechanical properties of individual electrospun fibers in tension have been measured using the AFM to apply force to the fibers whereas the SEM allows manipulation and observation of the electrospun fiber failure.[18] Such a setup can therefore be extended to examine the deformation behavior of two electrospun fibers connected together until sufficient force is applied using the AFM to separate the contacting fibers. We examine the cross-cylinder fiber contact geometry used in previous literature and additionally evaluate a parallel configuration that is more representative of the in-plane fiber-fiber contact within the network. These experiments will provide a quantitative insight into the adhesion between electrospun fibers in the network for membrane in-plane loading conditions commonly found in filtration and tissue engineering applications.

EXPERIMENTAL SECTION

Electrospinning. Production of electrospun polymer fibers was carried out by first dissolving solid polyamide 6 (PA6, Nylon 6, M_w = 24000 $gmol^{-1}$, BASF, Ultramid B33 L, Germany) in a mixture of acetic acid (≥99.7%, Sigma Aldrich, U.S.A.) and formic acid (98%, Sigma Aldrich, U.S.A.) (50/50 mass ratio) to produce a resultant polymer concentration of 12 wt% in solution. The PA6 polymer solution was electrospun into fibers using a large scale multi-jet electrospinning setup (NanoSpider, Elmarco, Czech Republic) as used previous.[15,19] An example of the electrospun PA6 fiber network is presented in Figure 1 and 2.

Attachment of individual electrospun fibers to AFM tips. Adhesion between two electrospun fibers was achieved by locating and isolating two individual fibers, designated fiber 1 and fiber

2, from the electrospun fiber network for subsequent direct adhesion testing between the two fibers. The attachment of individual fibers to an AFM tip was carried out in the chamber of a SEM (FEI Quanta 3D, U.S.A./E.U.) containing a custom built nanomanipulator (attoAFM II, attocube GmbH, Germany) based on previous methodologies.[20] A small section of the electrospun PA6 network was first placed onto carbon tape and attached to a sample stage holder within the SEM chamber. A small droplet of vacuum compatible glue (Poxipol, Argentina), initially in liquid form, was also added to the sample stage holder. An AFM tip for fiber 1 and 2 (Veeco, U.S.A., spring constant for fiber 1, $K_1 = 0.08$ N.m^{-1} and $K_2 = 41.6$ N.m^{-1} for fiber 2) was attached to the nanomanipulator system and the tip translated towards the glue while observing using the SEM as previously described.[21,22] Contact of the AFM tip with the droplet of glue within the SEM chamber caused deposition of the glue at the apex of the AFM tip. The AFM tip with glue was subsequently translated towards an individual electrospun fiber protruding from the edge of the network until contact between individual fiber and glue on the AFM tip occurred, as shown in Figure 3. Focus ion beam (FIB) microscopy integrated within SEM was used to section through the individual fiber fixed to the AFM tip from the electrospun network using a voltage U=30 kV and beam current of I=0.5 nA to give resultant free electrospun fiber lengths of approximately 10 μm attached to the AFM tip. The glue holding the individual electrospun fiber to the AFM tip cured towards the solid state after approximately 20 minutes, providing sufficient time to perform the manipulation process as shown in Figure 4. Two sets of fibers (fiber 1 and fiber 2) were attached to separate AFM tips with soft and stiff cantilevers respectively so that one AFM tip acted as a rigid grip whereas the second AFM tip used the softer cantilever to record the force applied to the adhesive contact between the electrospun fibers during the separation process, as has been utilized in tensile testing of fibrous nanomaterials.[18] The fibers were

attached with their principal axis perpendicular to the long length of the AFM cantilever and parallel to the AFM tip axis.

Adhesion testing. Measuring the adhesion between contacting fibers as shown in Figure 4 was performed using a setup where a custom built AFM was incorporated within an SEM chamber as described previously.[17,18] The soft cantilever system containing fiber 1 was placed in the AFM so that the cantilever deflection could be accurately determined and converted to force acting on fiber 1 using a low-coherence optical interferometer system situated behind the AFM cantilever.[20] The stiffer cantilever containing fiber 2 was placed onto the sample stage of the AFM system. The piezo positioners of the AFM system were used to move the fibers into contact with one another such as shown in Figures 4. SEM secondary electron imaging was applied in this initial experimental setup using electron beam conditions of 5 kV and 53.3 pA to measure the average fiber diameters of 300 ± 25 nm for fiber 1 and 420 ± 36 nm for fiber 2. The contact line between fibers for the parallel configuration in the adhesion test was varied in the experiments by translating a range of fiber lengths into contact with one another using the piezo positioners of AFM system. The contact length between parallel fibers was defined based on the schematics presented in Figure 4(d) and was measured from SEM images using IrfanView software (version 4.33, Austria). The measurement error for the contact length between fibers was ± 6 % due to the image resolution of the SEM.

Adhesion testing was achieved by translating fiber 1 away from fiber 2 as shown in Figure 4 in both cross-cylinder (Figure 4 (c)) and parallel (Figure 4 (d)) configurations using the z-piezo positioner of the AFM system. Note that a van der Waals snap in brings fibers into contact with

each other, which occurs when the manipulated fibers come into close proximity and thus do not require the AFM to apply a contacting force. This practice was applied for both fiber configurations in all adhesion tests.

Exposure of non-conductive samples to the electron beam can cause an accumulation of charge on the surface. A change in the deflection of the cantilever was observed when the electron beam was blanked after imaging the contact point between fibers. The change in deflection is due to the effects of an electrostatic field produced from charging of the fibers and cantilever by the electron beam. The cantilever deflection signal recorded by the AFM was therefore allowed to stabilize after beam blanking, which showed that the charge had dissipated. The minimum time for the charge dissipation to occur was observed as being 32 seconds, and a minimum of 90 seconds was allowed between imaging with the SEM and adhesion testing. These observations highlighted the need to first image the contacting electrospun fibers using SEM but perform separation experiments with the SEM electron beam blanked. Due to beam blanking during the adhesion tests, we were not able to record any changes of the contact between fibers that could occur because of fiber bending. The translational velocity when separating fiber 1 from fiber 2 was kept constant at 2.93 μms^{-1} for all adhesion experiments. An initial displacement was used to straighten the contacting electrospun fibers and remove bending effects, as carried out in previous work,[20] prior to adhesion testing. Translation of fiber 1 away from fiber 2 caused a linear increase in the force acting between the two fibers with displacement of the z-piezo positioner as shown in Figure 5.

The force acting on fiber 1 was sufficient to overcome the adhesion contact between fiber 2 at a critical displacement and separation occurred, indicated by a drop in the applied force acting between the fibers to the zero point. A total of 40 adhesion test measurements were carried out

with fiber 1 and fiber 2. The example of a recorded adhesion test movie, taken with the SEM for illustrative purposes, is presented in Supporting Information. No slippage between fibers was observed during the adhesion tests. The contact length between the fibers was at a range of points along each fiber length and, as the fiber diameters varied along their lengths, a range of contact dimensions were examined using this two fiber setup.

RESULTS AND DISCUSSION

The pull-off force needed to separate two contacting fibers is given by the maximum force obtained from force-displacement curves collected from AFM measurements, with an example curve displayed in Figure 5. The linear increase in force with displacement was observed for all parallel and cross-cylinder configurations. This linear relationship indicates a buildup of stress at the contact between the fibers until, at a critically applied force, complete separation of the fibers occurred and the force dropped to zero. Such an observation would indicate that frictional sliding is absent in our experiments. For a cross-cylinder fiber contact configuration, the measured pull-off forces are in the range of 0.188 to 0.513 μN. For the parallel configuration of fibers, the variation in contact length is expected to influence the recorded maximum force causes fiber separation, with an increasing contact length requiring a correspondingly increasing pull-off force. A plot of the pull-off force with contact length is shown in Figure 6. This maximum recorded pull-off force between the contacting PA6 fibers varied from 0.145 to 0.548 μN for contact lengths ranging from 0.413 to 0.778 μm. Moreover, Figure 6 indicates a trend of increasing pull-off force with increasing contact length.

Measurement of pull-off force and fiber-fiber contact length requires suitable interpretations of the experimental results. The most appropriate theory describing adhesion between soft bodies in elastic contact is either Johnson-Kendall-Roberts (JKR) theory[23] or Derjaguin-Muller-Toporov (DMT) theory[24]. Generally, JKR considers short range surface attractions and correlates the contact area between two soft bodies to their elastic properties and resultant interfacial interaction strength. DMT considers long range attractions for hard solids where van der Waals interactions are present outside the elastic contact regime. The selection of the most appropriate theory can be made according to the calculation of a dimensionless number based on the Tabor parameter μ_M[25,26]. Originally, μ_M was derived for spheres but has also been shown to be valid for cylindrical contacts such as presented in this work.[5] The Tabor parameter specifically suggests the use of JKR theory unless the limit for selecting DMT theory is reached where $\mu_M < 0.1$.[26] Calculation of μ_M is therefore required to evaluate the contact mechanics between individual electrospun fibers using the following:[25,26]

$$\mu_M = \left[\frac{16RW^2}{9E^{*2}z_o^3}\right]^{\frac{1}{3}} \quad (1)$$

where R is effective contact radius between two fibers of radii R_1 and R_2 such that $1/R=1/R_1+1/R_2$. W is work of adhesion between the fiber contacts, z_o is equilibrium separation of the surfaces equal to 1 nm,[5] E^* is the combined elastic modulus for two fibers where $1/E^*=(1-\nu_1^2)/E_1+(1-\nu_2^2)/E_2$ for the polyamide (PA6) fibers of this work with $\nu_1 = \nu_2 = 0.39$ [27], and $E_1 = E_2 =$ 418 MPa.[19] The Tabor parameter μ_M estimated from Equation 1 for the electrospun fiber contact is above 5, suggesting JKR should be more suitable in describing the fiber-fiber contact in cross-cylinder configuration as opposed to the limit of $\mu_M < 0.1$ for the application of DMT theory.[26] JKR theory is therefore applied to the adhesion tests in the cross-cylinder and parallel

configurations as shown in Figure 4. In particular, for a cross-cylinder configuration where the orientation of contacting fibers is assumed to occur at an angle θ, JKR theory is able to correlate the maximum pull-off force F_p to the work of adhesion, W, by:[5]

$$W_c = \frac{2F_p}{3\pi R_e} \tag{2}$$

where the effective contact radius $R_e = \sqrt{R_a R_b}$. This effective radius between two fibers is dependent on the angle θ made between the two fibers such that $R_a = R_1/(1-\cos\theta)$ and $R_b = R_2/(1+\cos\theta)$ and $R_1 > R_2$.[28] The effective contact radius can be simplified to $R_e \equiv \sqrt{R_1 R_2}$ when the fibers contact one another at $\theta = 90°$.[28,29]

The parallel configuration of fibers, where fibers contact each other along their principal axis as shown in Figure 4 (d-f), is given by the expression:[30]

$$W_p = \frac{\left[\left(\frac{3\pi K a^2 L}{8R}\right) - P\right]^2}{6\pi K a L^2} \tag{3}$$

where $K=4E^*/3$, $2L$ is the contact length, $P = 2LF_p$ and $2a$ is the width of the contact area between fibers as shown in Figure 4 (d). The width of the contact area in a parallel configuration has been found to be 1/3 of the $2R$ diameter for contact between cylinders[30], resulting in a contact area width of $2a$. We note that R and R_e can be considered as approximately equal when R_1 becomes similar to R_2. The work of adhesion between PA6 fibers in the cross-cylinder configuration was calculated from Equation 2 and ranged from 225 to 613 $mJ.m^{-2}$. The parallel configuration calculated from Equation 3 was 628 $mJ.m^{-2}$. All work of adhesion values for separating the pair of contacting fibers with a variety of contacts are summarized in Table 1.

Figure 7 displays the work of adhesion for the cross-cylinder and parallel fiber contacts, including the variability in the measurements. This variation in the work of adhesion between the electrospun fibers in a cross-cylinder configuration is substantial whereas there is considerably less variation in the work of adhesion for parallel contacting fibers, despite using a range of contact lengths in the separation experiments. The scatter in the cross-cylinder work of adhesion measurement is expected to be due to the angle between the contacting fibers deviating from the 90° configuration assumed by Equation 2. The angle made between the contacting fibers critically causes changes in the contact area, with elliptical contact of increasing area occurring as the fiber orientation deviates from the 90° cross-cylinder configuration. The idealized contact between fibers in a cross-cylinder configuration as shown in Figure 4(c) contains errors due to the SEM observations showing an angle of contact between fiber 1 and 2 varying by up to 30° from the assumed 90°. This deviation from the ideal cross-cylinder configuration is responsible for the error in the work of adhesion values shown in Figure 7. Parallel fiber contact is an inherently simpler system as the contact zone between the two fibers shown in Figure 4 (d) is a rectangular geometry as described using Equation 3.[30] The contact area between the fibers will increase with the contact length and produces a corresponding increase in the pull off force as shown in Figure 6. Importantly, the results for cross-cylinder configuration from our adhesion experiments are similar to previous tests[5,31] stating a work of adhesion of approximately 200 $mJ.m^{-2}$ for electrospun fibers contacting in a cross-cylinder configuration. This similarity between our results and previous literature for a cross-cylinder configuration validates the current experimental results and work of adhesion evaluation. Critically, the work of adhesion for fibers in the cross-cylinder configuration is lower than for the parallel fiber configuration

over a range of contact lengths. Our results therefore indicate adhesion anisotropy for contacting electrospun fibers, which highlights a need to quantify both the adhesion properties between contacting fibers and their contact orientation. The increase in the work of adhesion for the parallel fiber configuration relative to the cross-cylinder configuration is suggested as being due to polymer chain orientation in electrospun fibers. Specifically, electrospinning processes are known to cause orientation of polymer chains within electrospun fibers.[32,33] Contacting electrospun fibers in a parallel configuration will therefore cause overlap of polymer chains at these adjacent fiber surfaces. However, electrospun fibers in a cross-cylinder configuration will have less polymer chain overlap length due to polymer chains in one fiber oriented perpendicular to the polymer chains at the surface of the adjacent fiber. The net van der Waals force per unit area for the parallel configuration is thus expected to be larger than for the cross-cylinder configuration. Indeed, enhanced work of adhesion for oriented polymer chains due to increased net van der Waals interactions have been observed for molecular alignment in polymer films.[34] We therefore propose adhesion anisotropy as a product of the structural anisotropy produced from the electrospinning process.

CONCLUSIONS

An *in situ* AFM technique was used to manipulate individual electrospun fibers and measure the work of adhesion when separating individual electrospun PA6 fibers using a range of contact areas and orientations. Experiments provided information on both the contact length between the fibers using SEM and measurement of the pull-off force with AFM. A clear increase in the pull-off force with increasing contact length between electrospun fibers was observed in experiments when translating electrospun fibers along their fiber axis in a parallel contacting cylinder

geometry, which is representative of electrospun network deformation where loading occurs within the plane of the network. Resultant adhesion anisotropy was found due to an increase in the work of adhesion for separation of fibers in a parallel fiber configuration when compared to the cross-cylinder configuration. This increase in the work of adhesion for the parallel fiber configuration is proposed as being due to polymer chain orientation introduced from electrospinning process, which increases net van der Waals interactions along the principle axis of fiber. Our results highlight a need to evaluate the adhesion in electrospun fibrous networks, and indeed other nanofibrous systems where network properties are critically dependent on fiber-fiber contact, both in terms of the intrinsic material surface properties and extrinsic fiber orientation.

ASSOCIATED CONTENT

Supporting Information. Movie of adhesion experiment where a pair of individual electrospun PA6 fibers are separated using in situ AFM. This material is available free of charge via the Internet at http://pubs.acs.org.

AUTHOR INFORMATION

Corresponding Author

*E-mail: a.h.barber@qmul.ac.uk

Present Addresses

† National Engineering Research Center for Tissue Restoration and Reconstruction, South China University of Technology, Guangzhou 510640, PR China

Notes

The authors declare no competing financial interest.

ACKNOWLEDGMENTS

We thank Dr Zofia Luklinska at the Queen Mary NanoVision Centre for assistance with microscopy facilities.

REFERENCES

1. Halaui, R.; Moldavsky, A.; Cohen, Y.; Semiat, R.; Zussman, E. Development of Micro-Scale Hollow Fiber Ultrafiltration Membranes. *J. Membr. Sci.* **2011**, 379, 370-377.
2. Lowery, J. L.; Datta, N.; Rutledge, G. C. Effect of Fiber Diameter, Pore Size and Seeding Method on Growth of Human Dermal Fibroblasts in Electrospun Poly(Epsilon-Caprolactone) Fibrous Mats. *Biomaterials* **2010**, 31, 491-504.
3. Hakimi, O.; Murphy, R.; Stachewicz, U.; Hislop, S.; Carr, A. J. An Electrospun Polydioxanone Patch for the Localisation of Biological Therapies During Tendon Repair. *Eur. Cells Mater.* **2012**, 24, 344-57.
4. Buell, S.; Rutledge, G. C.; Van Vliet, K. J. Predicting Polymer Nanofiber Interactions Via Molecular Simulations. *ACS Appl. Mat. Inter.* **2010**, 2, 1164-1172.
5. Shi, Q. A.; Wan, K. T.; Wong, S. C.; Chen, P.; Blackledge, T. A. Do Electrospun Polymer Fibers Stick? *Langmuir* **2010**, 26, 14188-14193.
6. Shi, Q.; Wong, S.-C.; Ye, W.; Hou, J.; Zhao, J.; Yin, J. Mechanism of Adhesion between Polymer Fibers at Nanoscale Contacts. *Langmuir* **2012**, 28, 4663-4671.
7. Wang, X.; Najem, J. F.; Wong, S.-C.; Wan, K.-t. A Nano-Cheese-Cutter to Directly Measure Interfacial Adhesion of Freestanding Nano-Fibers. *J. Appl. Phys.* **2012**, 111, 024315-6.
8. Lee, J.; Fearing, R. S.; Komvopoulos, K. Directional Adhesion of Gecko-Inspired Angled Microfiber Arrays. *Appl. Phys. Lett.* **2008**, 93, 191910-3.
9. Autumn, K.; Majidi, C.; Groff, R. E.; Dittmore, A.; Fearing, R. Effective Elastic Modulus of Isolated Gecko Setal Arrays. *J. Exp. Biol.* **2006**, 209, 3558-3568.

10. Arinstein, A.; Burman, M.; Gendelman, O.; Zussman, E. Effect of Supramolecular Structure on Polymer Nanofibre Elasticity. *Nat. Nanotechnol.* **2007**, 2, 59-62.

11. Gillies, A. G.; Fearing, R. S. Shear Adhesion Strength of Thermoplastic Gecko-Inspired Synthetic Adhesive Exceeds Material Limits. *Langmuir* **2012**, 27, 11278-11281.

12. Good, R. J. Contact Angle, Wetting, and Adhesion: A Critical Review. *J. Adhes. Sci. Technol.* **1992**, 6, 1269-1302.

13. Ma, M. L.; Mao, Y.; Gupta, M.; Gleason, K. K.; Rutledge, G. C. Superhydrophobic Fabrics Produced by Electrospinning and Chemical Vapor Deposition. *Macromolecules* **2005**, 38, 9742-9748.

14. Salas, C.; Genzer, J.; Lucia, L. A.; Hubbe, M. A.; Rojas, O. J. Water-Wettable Polypropylene Fibers by Facile Surface Treatment Based on Soy Proteins. *ACS Appl. Mat. Inter.* **2013**, 5, 6541-6548.

15. Stachewicz, U.; Modaresifar, F.; Bailey, R. J.; Peijs, T.; Barber, A. H. Manufacture of Void-Free Electrospun Polymer Nanofiber Composites with Optimized Mechanical Properties. *ACS Appl. Mat. Inter.* **2012**, 4, 2577–2582.

16. Tajparast, M.; Glavinovic, M. I. Forces and Stresses Acting on Fusion Pore Membrane During Secretion. *BBA-Biomembranes* **2009**, 1788, 1009-1023.

17. Stella, J. A.; Wagner, W. R.; Sacks, M. S. Scale-Dependent Fiber Kinematics of Elastomeric Electrospun Scaffolds for Soft Tissue Engineering. *J. Biomed. Mater. Res. A* **2010**, 93A, 1032-1042.

18. Yu, M. F.; Lourie, O.; Dyer, M. J.; Moloni, K.; Kelly, T. F.; Ruoff, R. S. Strength and Breaking Mechanism of Multiwalled Carbon Nanotubes under Tensile Load. *Science* **2000**, 287, 637-640.

19. Stachewicz, U.; Peker, I.; Tu, W.; Barber, A. H. Stress Delocalization in Crack Tolerant Electrospun Nanofiber Networks. *ACS Appl. Mat. Inter.* **2011**, 3, 1991-1996.

20. Hang, F.; Lu, D.; Bailey, R. J.; Jimenez-Palomar, I.; Stachewicz, U.; Cortes-Ballesteros, B.; Davies, M.; Zech, M.; Boedefeld, C.; Barber, A. H. In Situ Tensile Testing of Nanofibers by Combining Atomic Force Microscopy and Scanning Electron Microscopy. *Nanotechnology* **2011**, 22, 365708-8.

21. Stachewicz, U.; Stone, C. A.; Willis, C. R.; Barber, A. H. Charge Assisted Tailoring of Chemical Functionality at Electrospun Nanofiber Surfaces. *J. Mater. Chem.* **2012**, 22, 22935-22941.

22. Stachewicz, U.; Barber, A. H. Enhanced Wetting Behavior at Electrospun Polyamide Nanofiber Surfaces. *Langmuir* **2011**, 27, 3024-3029.

23. Johnson, K. L.; Kendall, K.; Roberts, A. D. Surface Energy and the Contact of Elastic Solids. *P. Roy. Soc. Lond. A Mat.* **1971**, 324, 301-313.

24. Derjaguin, B. V.; Muller, V. M.; Toporov, Y. P. Effect of Contact Deformations on Adhesion of Particles. *J. Colloid Interf. Sci.* **1975**, 53, 314-326.

25. Maugis, D. Adhesion of Spheres: The Jkr-Dmt Transition Using a Dugdale Model. *J. Colloid Interf. Sci.* **1992**, 150, 243-269.

26. Carpick, R. W.; Agrait, N.; Ogletree, D. F.; Salmeron, M. Variation of the Interfacial Shear Strength and Adhesion of a Nanometer-Sized Contact. *Langmuir* **1996**, 12, 3334-3340.

27. Wang, J.-J.; Chang, T.-P.; Chen, B.-T.; Lin, H.-C.; Wang, H. Evaluation of Resonant Frequencies of Solid Circular Rods with Impact-Echo Method. *J. Nondestruct. Eval.* **2010**, 29, 111-121.

28. Suemer, B.; Onal, C. D.; Aksak, B.; Sitti, M. An Experimental Analysis of Elliptical Adhesive Contact. *J. Appl. Phys.* **2010**, 107, 113512-7.

29. Wu, J.-J. Numerical Analyses on Elliptical Adhesive Contact. *J. Phys. D Appl. Phys.* **2006**, 39, 1899-1907.

30. Chaudhury, M. K.; Weaver, T.; Hui, C. Y.; Kramer, E. J. Adhesive Contact of Cylindrical Lens and a Flat Sheet. *J. Appl. Phys.* **1996**, 80, 30-37.

31. Na, H.; Chen, P.; Wan, K.-T.; Wong, S.-C.; Li, Q.; Ma, Z. Measurement of Adhesion Work of Electrospun Polymer Membrane by Shaft-Loaded Blister Test. *Langmuir* **2012**, 28, 6677-6683.

32. Stachewicz, U.; Bailey, R. J.; Wang, W.; Barber, A. H. Size Dependent Mechanical Properties of Electrospun Polymer Fibers from a Composite Structure. *Polymer* **2012**, 53, 5132-5137.

33. Camposeo, A.; Greenfeld, I.; Tantussi, F.; Pagliara, S.; Moffa, M.; Fuso, F.; Allegrini, M.; Zussman, E.; Pisignano, D. Local Mechanical Properties of Electrospun Fibers Correlate to Their Internal Nanostructure. *Nano Letters* **2013**, 13, 5056-5062.

34. Stachewicz, U.; Li, S.; Bilotti, E.; Barber, A. H. Dependence of Surface Free Energy on Molecular Orientation in Polymer Films. *Appl. Phys. Lett.* **2012**, 100, 094104-4.

Figures:

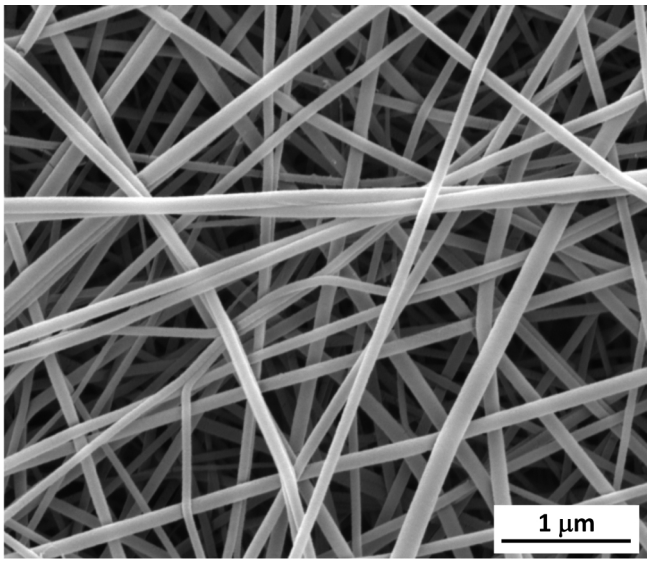

Figure 1. Scanning electron micrograph of electrospun Nylon 6 fibers.

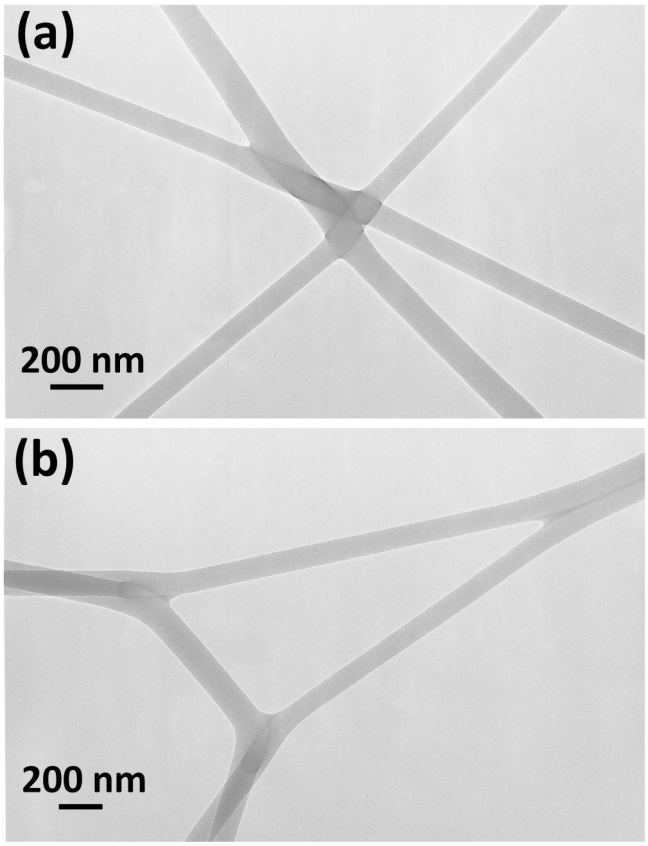

Figure 2. Transmission electron micrographs of electrospun Nylon 6 fibers indicating contact between fibers in a membrane.

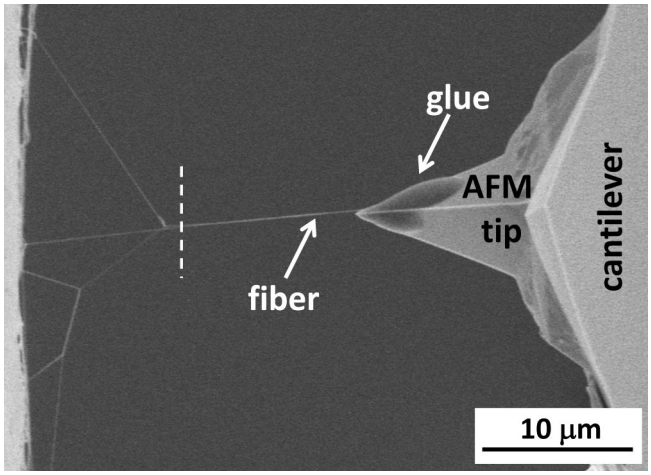

Figure 3. Scanning electron micrograph of the AFM tip with glue in contact with an individual electrospun PA6 fiber protruding from the electrospun mat. The dashed line indicates the FIB sectioning carried out to isolate a fiber free length from the electrospun membrane.

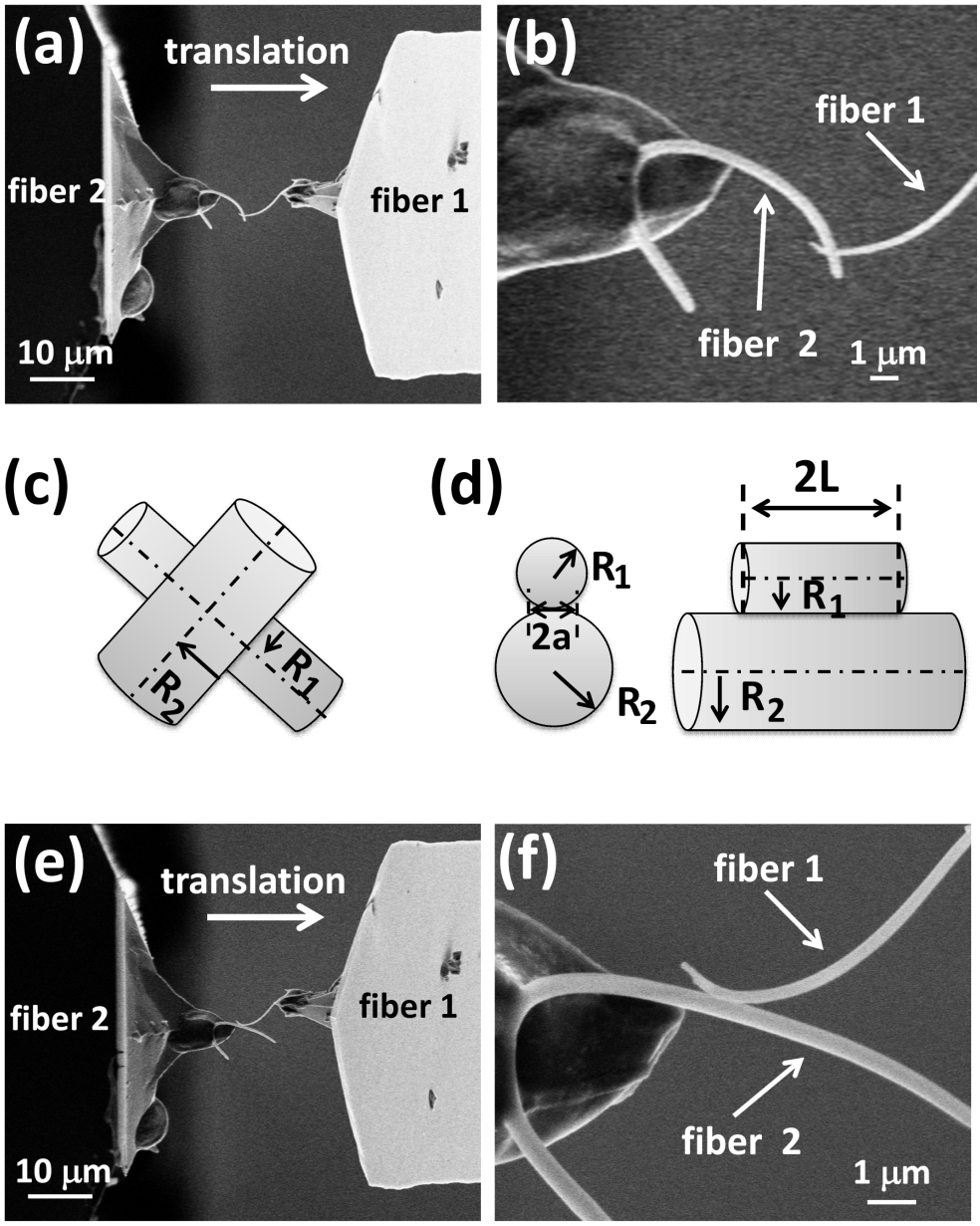

Figure 4. Scanning electron micrographs showing a typical experiment where (a) two individual electrospun fibers contact one another in a cross-cylinder configuration (b) a higher magnification image provides evidence of the contact between the individual fibers (c) schematic of a cross-cylinder configuration (d) schematic of a parallel configuration and examples of contact length, L, measurement between fiber 1 with a radius of R_1 and fiber 2 with radius R_2 exhibiting a contact width between fibers of $2a$ (e) typical experiment showing fiber 1 contacting

the lower surface of fiber 2 in a parallel configuration and (f) contact between the individual fibers observed at higher magnification.

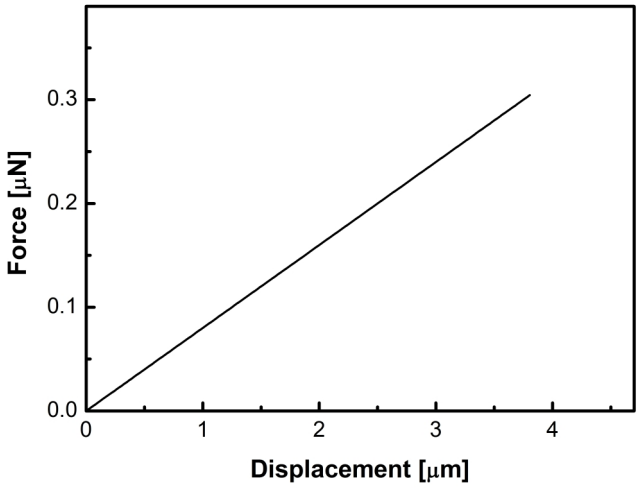

Figure 5. A representative plot of the increase in force applied to two contacting electrospun PA6 fibers with increasing z-piezo positioner displacement used to separate the contacting electrospun fibers.

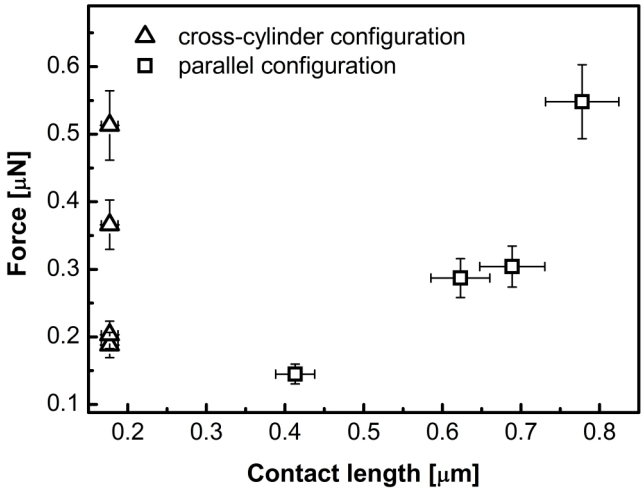

Figure 6. Measured pull-off force required to separate two individual electrospun PA6 fibers in parallel configuration for a given contact length L and for cross-cylinder configuration at the contact $R_e = 0.177$ μm.

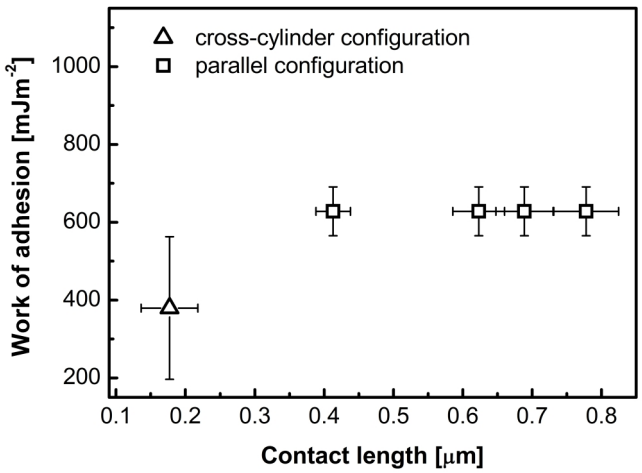

Figure 7. Variation in the work of adhesion values for electrospun fibers with contact length for parallel and cross-cylinder configurations. Cross-cylinder configurations provide a fixed contact length whereas a range of contact lengths are produced for the parallel fiber configurations.

Tables:

Table 1. Pull-off force and work of adhesion for separating PA6 fibers in minimum contact area between fibers in cross-cylinder configuration defined by R_e according to the Eq. 2 and of specific contact length for parallel configuration.

Test	Fiber contact configuration	Contact length L [μm]	Measured force F [μN]	Work of adhesion W [mJm^{-2}]
1	cross-cylinder	-	0.366	437
2	cross-cylinder	-	0.188	224
3	cross-cylinder	-	0.203	242
4	cross-cylinder	-	0.513	613
5	parallel	0.413	0.145	628
6	parallel	0.689	0.304	628
7	parallel	0.623	0.287	628
8	parallel	0.778	0.548	628

"TOC graphic" - Table of contents only